Electronic Supplementary Material (ESI) for Physical Chemistry Chemical Physics.
This journal is © the Owner Societies 2019

Dimethylaniline Functionalised Pyrene Fluorophores; Dual Colour Switching in Solution and Self-Assembled Monolayers.

Darragh O' Connor[a], Carolin Müeller[b], Nirod Sarangi[a], Aisling Byrne[a] and Tia E. Keyes[a]*

[a]School of Chemical Sciences and National Centre for Sensor Research, Dublin City University, Glasnevin, Dublin 9, Ireland.

[b] Friedrich-Schiller-University Jena, Institute for Physical Chemistry, Helmholtzweg 4, 07743 Jena.

*Corresponding author

Supplementary Information

Experimental Section

Materials and Instrumentation

All chemical reagents were purchased from Sigma Aldrich (Ireland) and used without further purification unless otherwise stated.

Instrumentation

^{1}H and ^{13}C NMR spectra were recorded on a 400 MHz or 600 MHz Bruker spectrometer respectively and the solvent stated. The spectra were processed using Bruker Topspin NMR software. High Resolution Mass Spectrometry (HR-MS) was carried out at the Mass Spectrometry facility, University College Dublin. MALDI-ToF mass spectrometry was performed on MALDI-Q-ToF Premier instrument at Trinity College Dublin. Elemental analysis was carried out using an Exeter Analytical CE 440 elemental analyser at the Microanalytical Laboratory, University College Dublin. Analytical HPLC was performed on a Varian 940-LC Liquid Chromatograph using an Agilent Pursuit XRs 5C-C18 column (4.6x250 mm) and the solvent system stated. Flow rates were kept at 1.6 mL/min and run times were 20 minutes. PDAD was used for peak detection and the analysis was followed by monitoring 280 nm and 430 nm channels. UV – Vis absorption spectra were recorded on Varian Cary 50 spectrometer. Samples were analysed in Hellma quartz fluorescence cuvettes, with a path length of 1 cm, and spectral range of 330 – 800 nm unless otherwise stated. Background measurements were carried out at room temperature prior to each measurement. Emission Spectra were recorded on a Varian Cary Eclipse fluorescence spectrophotometer with excitation and emission slit widths stated. All analyses were carried out using quartz cuvettes and background correction was applied prior to measurement. Fluorescence lifetime measurements were carried out using a PicoQuant FluoTime 100 Compact FLS TCSPC system using a 450 nm pulsed laser source generated from a PicoQuant PDL800-B box. The instrument response function was determined using Ludox colloidal silica solution. Lifetime decay plots were analysed using PicoQuant TimeHarp software. The goodness of each fit to exponential decay kinetics was assessed from chi – squared values (where χ^2 <1.3) and visual inspection of residuals.

Absorption and Fluorescence Measurements

UV-Vis spectra were recorded on a Varian Cary 50 spectrometer. Samples were analysed in Hellma quartz fluorescence cuvettes, with a path length of 1 cm, and spectral range of 280–800 nm unless otherwise stated. Background measurements were carried out at room temperature prior to each measurement. Solution phase emission Spectra were recorded on a Varian Cary Eclipse fluorescence spectrophotometer with excitation and emission slit widths as stated. All analyses were carried out using quartz cuvettes and background correction was applied prior to measurement. 77 K emission spectra were obtained a Varian Cary Eclipse fluorescence spectrophotometer using concentrations of 1 µM using excitation slit widths 5 nm and emission slit widths 10 nm over a spectral range of 440-800 nm. For pH-dependent experiments in solution, aqueous samples were prepared using phosphate buffer solution (PBS) with sample concentrations 100 µM, and they were titrated by successive of small volumes (in the order of microliters) of HCl and NaOH solutions (1 M) to an initial

volume of 5 mL for negligible changes to concentration and volume of the sample. pH of the samples was then measured using an EDT microprocessor pH meter.

For pH-dependent experiments in organic solution, samples in acetonitrile were prepared with sample concentrations 50 µM, and they were titrated by successive small volumes (in the order of microliters) of perchloric acid and triethylamine solutions of differing concentrations (0.5 – 1 M) to an initial volume of 5 mL for negligible changes to concentration and volume of the sample. pH of the samples was then calculated to obtain an apparent pH in organic solution. For studies of interfacial fluorescence of PyLaOT bound to gold, an Olympus confocal microscope attached to a Horiba Jobin-Y Labram HR 1000 spectrometer with a 50× long distance magnification objective (NA 0.55) was used. The excitation light of 458.7 nm was delivered by an Argon Ion Laser (Horiba Jobin-Y Labram HR 1000 (. The quantum yields of the samples ϕ_x were measured in solutions applying a standard reference of fluorescein in EtOH (ϕ_s = 0.79) and using equation 1,

$$\Phi_x = \Phi_s \cdot \frac{I_x}{I_s} \cdot \frac{A_s}{A_x} \cdot \frac{\eta_x^2}{\eta_s^2} \qquad (1)$$

where *I* is the integrated emission, *A* is the absorbance at the excitation wavelength and the subscripts *x* and *s* are the sample and standard, respectively. The refractive index of is given by *η.* The excitation and emission slit widths were both set to 5 nm.

Self-assembled Monolayer Formation of PyLaOT on Gold Electrode

Prior to self-assembled monolayer (SAM) modification, electrochemical cleaning procedure was carried out in 0.5 M H_2SO_4 from -0.2 to +1.6 V at 50 mV s-1 until reproducible voltammograms were obtained. Next, the electrode was rinsed with deionised (DI) water and finally dried by high pure stream of N_2. For the SAM modification, the electrode was immersed in the freshly prepared 1 mM PyLaOT in ethanolic solution for 48 hours. Upon removal, the electrode was washed with a copious amount of ethanol followed by DI water, and immediately transferred to the electrochemical cell for measurement.

Electrochemical Measurements

Cyclic voltammetry was carried out using a conventional three-electrode cell using 1 mM $[Fe(CN)_6]^{3-/4-}$ as an internal redox probe in 0.1 M KCl electrolyte solution in PBS buffer with an applied potential in the range of -0.2 to +0.8 V at a scan rate of 50 mV s^{-1}. The electrodes are gold (working electrode), Ag/AgCl (reference electrode) and platinum wire (counter electrode). Electrochemical impedance measurements were performed on a CHI 760B bipotentiostat (CH Instruments Inc., Austin, TX) in a three-electrode cell. The EIS recording was performed in the frequency region between 104 and 0.01 Hz with a bias potential of 0.26 V vs Ag/AgCl when redox probe is used and a bias potential of 0 V vs Ag/AgCl without

the redox probe i.e., only on PBS buffer. The EIS data were fit to equivalent circuit using Z view (v. 3.4e, Scribner Associates, Inc.)

Computation

The structural and electronic data of the pyrene derivatives (PyLa and its mono-, di- and triple protonated species) were obtained from quantum chemistry calculations performed with the Gaussian09 program.[1] The optimised equilibrium geometries and vibrational frequencies of the ground state were calculated by means of DFT with the hybrid-functional B3LYP[2,3] in cooperation with the triple-ζ-valence-polarization (TZVP) basis set.[4–6] Subsequent vibrational analysis confirmed that all obtained optimised structures correspond to a minimum on the potential energy hypersurface. The vertical excitation energies and oscillator strengths within the Franck-Condon region were obtained from TDDFT calculations by means of the 20 lowest singlet excited states. The TDDFT calculations were performed with four functionals, which include different amounts of Hartree-Fock exchange: B3LYP (20%), PBE0 (25%)[7–9], M06-2X (54%)[10] and CAM-B3LYP (19-65%)[11]; in cooperation with the TZVP basis set. The effects of solvation (Acetonitrile: ε=35.69, n=1.3442) on the ground and excited state properties were considered based on the integral equation formalism of the polarizable continuum model (IEFPCM).[12] In order to describe the influence of different protonation states of PyLa (*e.g.* first protonation in either the 3-, 6- or 8-position of the pyrene) on the absorption properties (as a mixture of several single or double-protonated forms, which can be present at room temperature) the oscillator strengths were statistically weighted using the Boltzmann distribution,

$$p_i = exp\left(-\frac{E_i}{k_B T}\right) \cdot \left[\sum_i^4 \exp\left(-\frac{E_i}{k_B T}\right)\right]^{-1}$$

where p_i is the weight and E_i the energy of a species *i* contributing to the absorption properties, k_B the Boltzmann constant and T the temperature.

Synthesis and Structural Characterisation

Synthesis of PyLa (1)

Was synthesised as previously reported[13].

Synthesis of PyLaOT (2)

DMF (5 mL) was purged with nitrogen for 20 minutes. To a reaction mixture of PyLa (**1**) (50 mg, 0.083 mmol), PyBOP (86 mg, 0.166 mmol) and DIPEA (60 uL), 8-aminooctanethiol hydrochloride (32 mg, 0.166 mmol) in 1 mL DMF was added slowly to the reaction mixture under nitrogen over a period of 30 minutes after which point the reaction mixture was allowed to stir at room temperature under nitrogen overnight. Following this the reaction mixture was precipitated using ice-cold water, collected under vacuum filtration and rinsed with ice-cold water (2 x 50 mL) and ice-cold MeOH (2 x 100 mL). The crude product was purified on silica gel by column chromatography eluent: Diethyl ether/DCM (80:20), dried over anhydrous Na_2SO_4 and concentrated to dryness under vacuum. Following this the compound was triturated using hot $CHCl_3$ and ice-cold MeOH to give the product. Yield: yellow-brown solid, 32.8 mg (0.043 mmol, 53 %).

^{1}H NMR (600 MHz, $CDCl_3$) (ppm): 8.45 (d, J = 9.5 Hz, 1H); 8.35 (d, J = 9.5 Hz, 1H); 8.27 (d, J = 10 Hz, 1H); 8.16 (d, J = 9.5 Hz, 1H); 8.03 (d, J = 2 Hz, 2H); 7.57-7.51(m, 6H); 6.91-6.89 (m, 6H); 6.13 (t, J = 5.5 Hz, 1H); 3.59 (q, J =11.5 Hz, 7.2 Hz Hz, 2H); 3.069 (s, 6H); 3.057 (s, 6H); 3.050 (s, 6H); 2.50 (q, J =16.5, 8 Hz, 2H); 1.71-1.66 (m, 2H); 1.62-1.57 (m, 2H); 1.46-1.27 (m, 11H).

^{13}C NMR (150 MHz, $CDCl_3$) (ppm): 170.35, 149.87, 138.26, 138.05, 136.77, 131.49, 131.31, 130.46, 129.89, 129.04, 128.69, 127.63, 127.38, 126.65, 126.60, 126.23, 126.03, 124.56, 123.51, 112.40, 40.67, 40.28, 34.02, 31.45, 30.21, 29.79, 29.71, 29.19, 28.98, 28.30m 26.96, 24.63, 14.13.

MADLI-TOF) m/z: calculated for $C_{49}H_{54}N_4OS$ 747.3998 found 746.4018 ([M+])

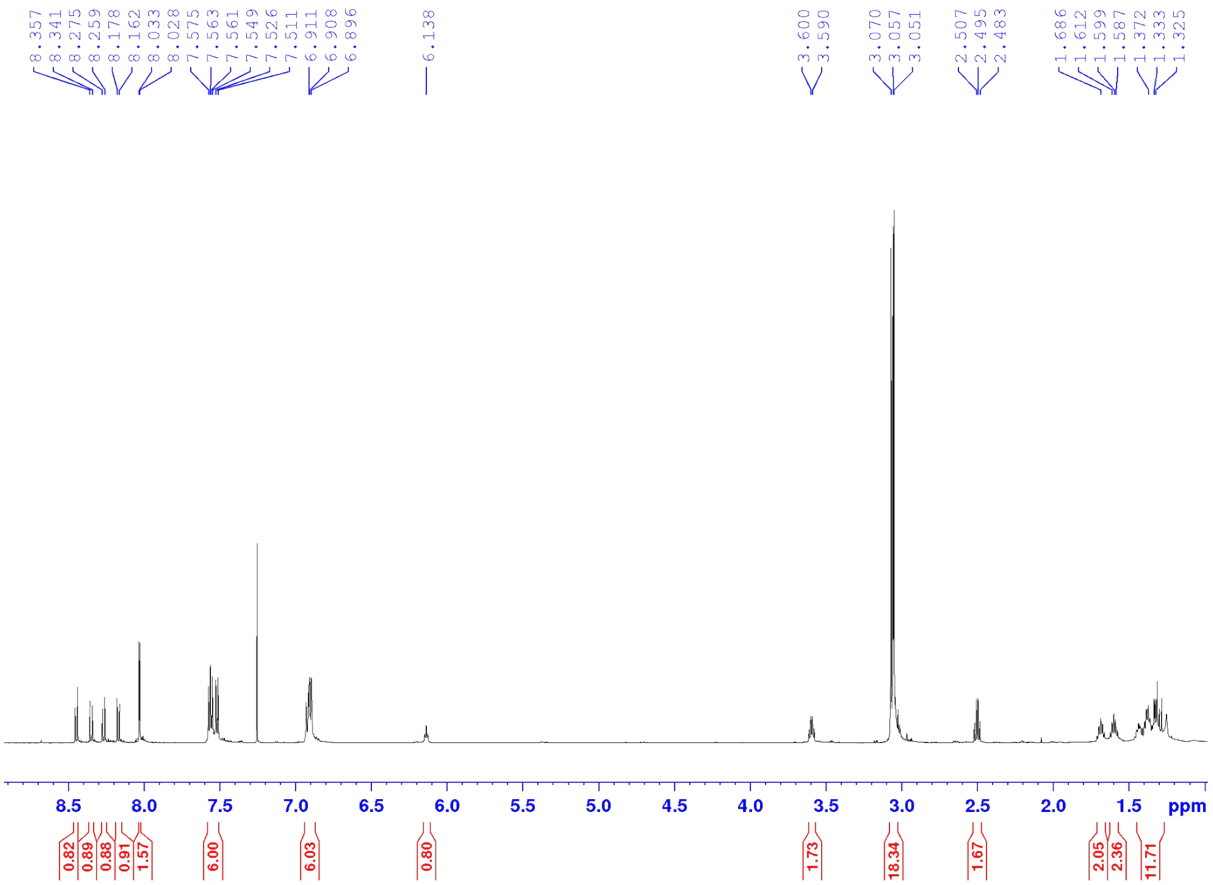

Figure S1 ^{1}HNMR (600 MHz) of PyLaOT (**2**) in $CDCl_3$.

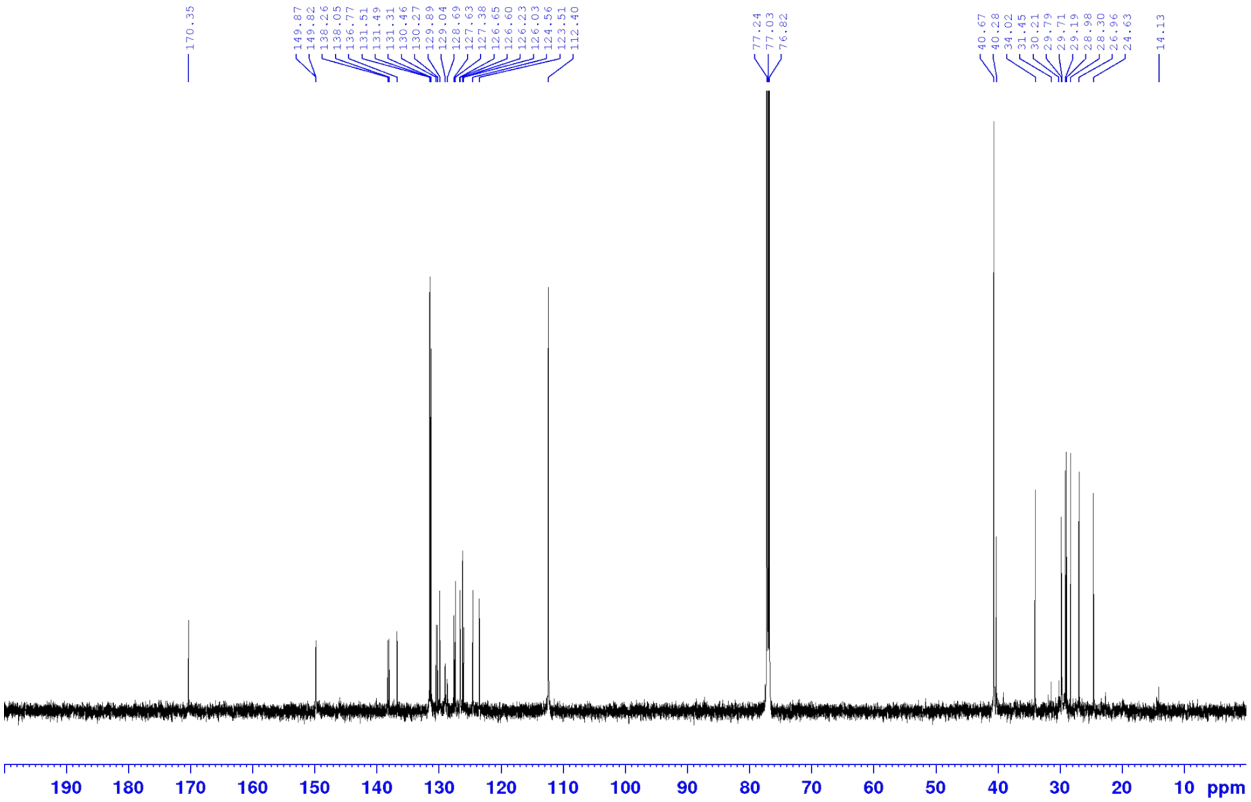

Figure S2 ^{13}CNMR (150 MHz) of PyLaOT (**2**) in $CDCl_3$.

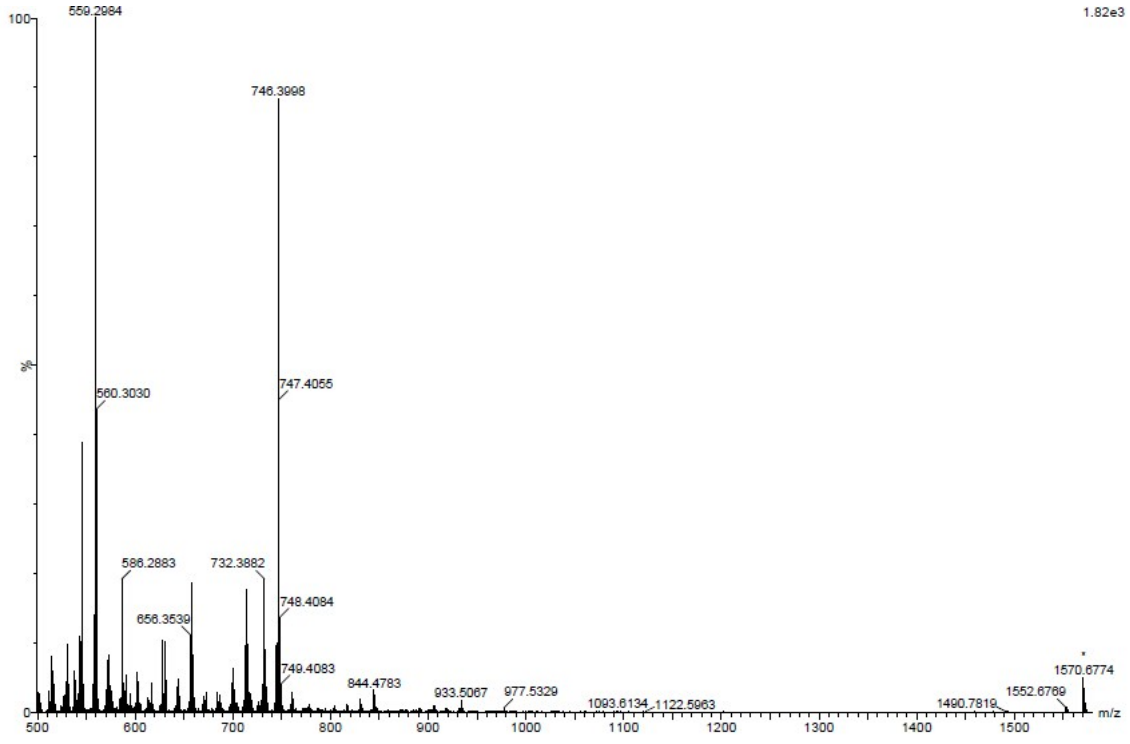

Figure S3 HR-MS (ESI-QTOF): Single Mass Analysis of PyLaOT indicating [M]+.

Single Mass Analysis
Tolerance = 50.0 PPM / DBE: min = -1.5, max = 400.0
Element prediction: Off
Number of isotope peaks used for i-FIT = 5

Monoisotopic Mass, Odd and Even Electron Ions
10 formula(e) evaluated with 1 results within limits (up to 10 best isotopic matches for each mass)
Elements Used:
C: 0-49 H: 0-54 N: 0-4 O: 0-1 S: 0-1

Darragh O'Connor (TK), PyLa-Ot
Q-TOF20180820MF010 56 (1.139) AM (Cen,6, 80.00, Ht,10000.0,1570.68,0.70); Sm (SG, 2x3.00); Sb (15,10.00); Cm (6:65-(55:58+62))

TOF MS LD+
1.61e+003

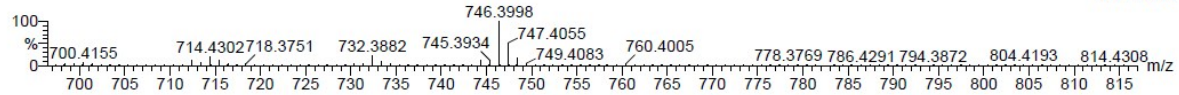

Minimum:				-1.5			
Maximum:		5.0	50.0	400.0			
Mass	Calc. Mass	mDa	PPM	DBE	i-FIT	i-FIT (Norm)	Formula
746.3998	746.4018	-2.0	-2.7	25.0	54.7	0.0	C49 H54 N4 O S

Figure S4 HR-MS (ESI-QTOF): Single Mass Analysis of PyLaOT indicating [M]+.

Computational Studies

Table S1 Electronic character, vertical excitation energies and oscillator strengths of the bright singlet excitations contributing to the UV-vis absorption properties of PyLa obtained at TD-DFT level of theory (CAM-B3LYP/TZVP) including the solvent effects of acetonitrile based on the integral equation formalism of the polarizable continuum model.

state	transition	P in %	E in eV	λ in nm	f	λ^{exp} in nm
S_1	$\pi_{8,py}$ (160) →$\pi^*_{9,py}$ + π^*_{COO}(161)	91	2.99	415	1.062	429
S_2	$\pi_{3,ph(2)}$ (159) →$\pi^*_{9,py}$ + π^*_{COO}(161)	45	3.57	347	0.131	370
	$\pi_{6,py}$ (156) → $\pi^*_{9,py}$ + π^*_{COO}(161)	21				
S_4	$\pi_{8,py}$ (160) → $\pi^*_{10,py}$ + π^*_{COO}(162)	36	3.85	322	0.540	300
	$\pi_{3,ph(2)}$ (159) →$\pi^*_{9,py}$ + π^*_{COO}(161)	32				
S_7	$\pi_{6,ph(2)}$ (156) →$\pi^*_{9,py}$ + π^*_{COO}(161)	39	4.49	276	0.467	265
	$\pi_{8,py}$ (160) → $\pi^*_{10,py}$ + π^*_{COO}(162)	22				

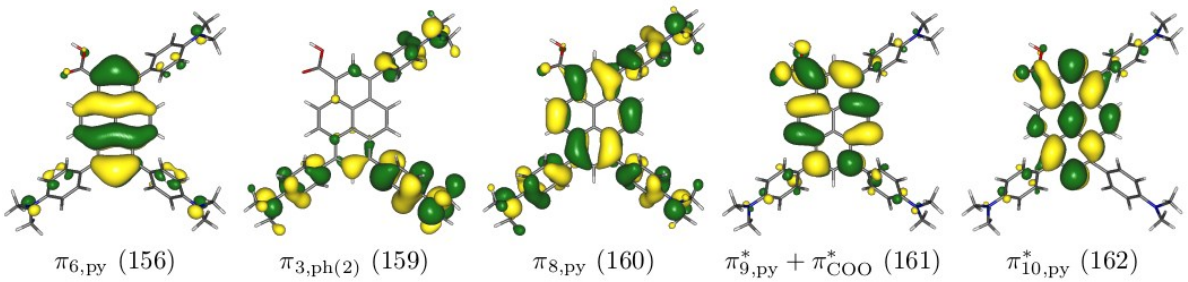

Figure S5 Isocontour representations (ρ = ±0.02) of the Kohn-Sham orbitals involved in the main configurations of the low-lying energetic states of PyLa (B3LYP/TZVP//TD-CAM-B3LYP/TZVP in the IEFPCM of acetonitrile), which are responsible for the ground state absorption properties.

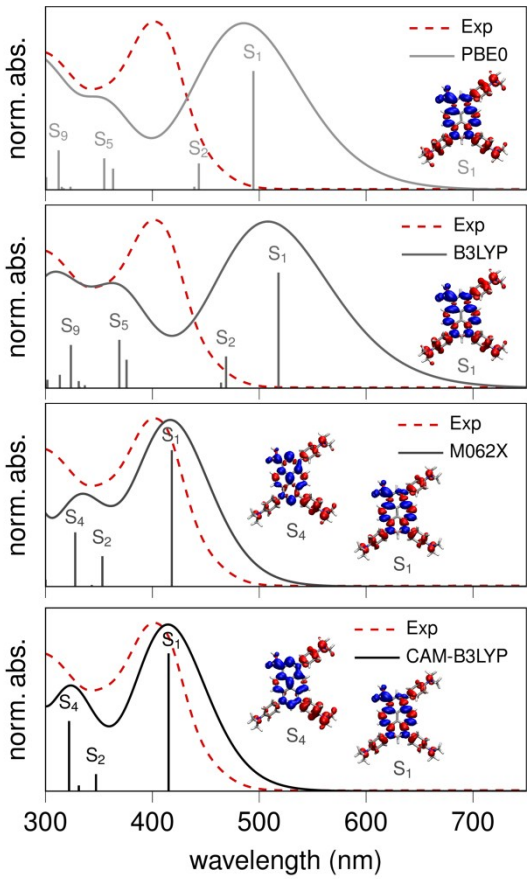

Figure S6 Experimental and simulated absorption spectra of PyLa. The vertical excitation energies are obtained from TD-DFT simulations on CAM-B3LYP/TZVP, M062X/TZVP, B3LYP/TZVP and PBE0/TZVP level of theory using a DFT (B3LYP/TZVP) optimised structure of the ground state. Some charge density differences of low-lying energetic states obtained for the different computational levels are depicted in the graphs (The excitation is from red (ρ = −0.005) to blue (ρ = +0.005).). Because the experimental absorption spectrum of PyLa in acetonitrile is described best using the CAM-B3LYP hybrid functional simulations of the mono-, di- and tris-protonated forms were performed on this level of theory.

Table S2 Calculated ground state energies (B3LYP/TZVP) of three different mono- (PyLa13, PyLa16 and PyLa18) and di-protonated forms (PyLa236, PyLa238 and PyLa268) of PyLa and their corresponding Boltzmann factors at room temperature.

Species	Relative energy	Boltzmann factor
Mono-protonated PyLa		
Py13	0.00 kJ/mol	0.369
Py16	0.55 kJ/mol	0.296
Py18	0.24 kJ/mol	0.335
Di-protonated PyLa		
Py236	1.08 kJ/mol	0.287
Py238	1.26 kJ/mol	0.268
Py268	0.00 kJ/mol	0.445

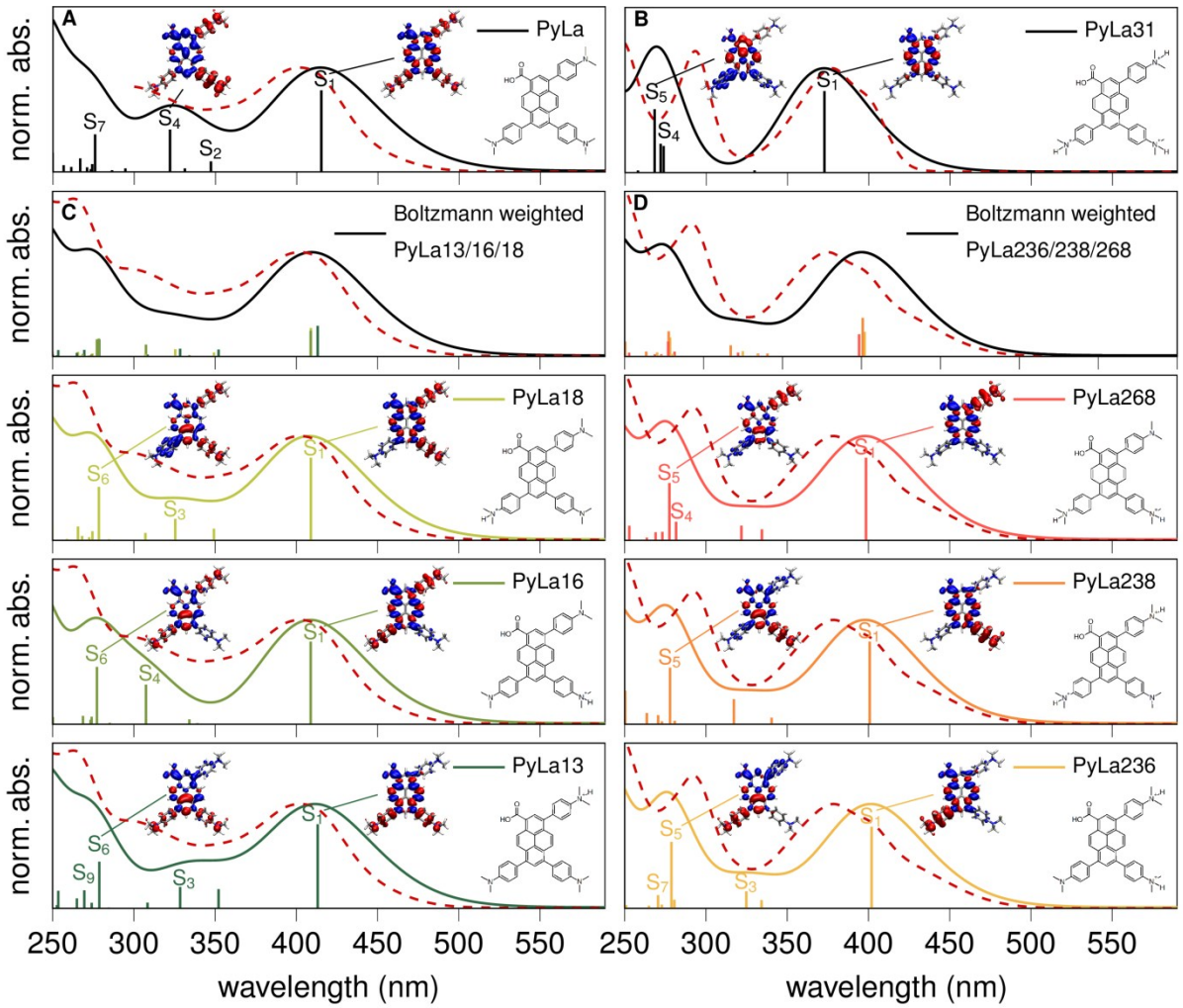

Figure S7 Experimental (red, dashed) and simulated (TD-CAM-B3LYP/TZVP) absorption spectra of PyLa (**A**) and three of its mono- (**C**: PyLa13, PyLa16, PyLa18) and di-protonated forms (**D**: PyLa236, PyLa238, PyLa268) as well as its tris-protonated species (PyLa31, **B**). Some charge density differences ($\rho = \pm 0.005$) of low-lying energetic states obtained for the different protonated species are depicted as inset (excitation from red to blue). For the mono- and di-protonated species the Boltzmann weighted absorption spectra are depicted in **C** and **D**.

Table S3 Calculated vertical excitation energies (E), oscillator strengths (f) and main single-excited configurations of the main excited states of the neutral PyLa species atB3LYP/TZVP//CAM-B3LYP/TZVP (IEFPCM of acetonitrile) as level of theory and experimental absorption maxima.

S_n	transition			p	E	λ	f	$\lambda^{\mathrm{Exp.}}$
				in %	in eV	in nm		in nm
			PyLa					
S_1	$\pi_{8,\mathrm{py}}$ (160)	$\rightarrow$	$\pi^*_{9,\mathrm{py}} + \pi^*_{\mathrm{COO}}$ (161)	91	2.99	415	1.062	429
S_4	$\pi_{8,\mathrm{py}}$ (160)	$\rightarrow$	$\pi^*_{10,\mathrm{py}} + \pi^*_{\mathrm{COO}}$ (162)	36	3.85	322	0.540	300
	$\pi_{3,\mathrm{DMA(2)}}$ (159)	$\rightarrow$	$\pi^*_{9,\mathrm{py}} + \pi^*_{\mathrm{COO}}$ (161)	32				
S_7	$\pi_{6,\mathrm{py}}$ (156)	$\rightarrow$	$\pi^*_{9,\mathrm{py}} + \pi^*_{\mathrm{COO}}$ (161)	39	4.49	276	0.467	265
	$\pi_{8,\mathrm{py}}$ (160)	$\rightarrow$	$\pi^*_{10,\mathrm{py}} + \pi^*_{\mathrm{COO}}$ (162)	22				
			PyLa03					
S_1	$\pi_{8,\mathrm{py}}$ (160)	$\rightarrow$	$\pi^*_{9,\mathrm{py}} + \pi^*_{4,\mathrm{DMA(3)}}$ (161)	90	3.28	378	1.092	360
S_3	$\pi_{3,\mathrm{DMA(6,8)}}$ (159)	$\rightarrow$	$\pi^*_{9,\mathrm{py}} + \pi^*_{4,\mathrm{DMA(3)}}$ (161)	71	4.06	306	0.686	300
S_6	$\pi_{8,\mathrm{py}}$ (160)	$\rightarrow$	$\pi^*_{4,\mathrm{DMA(3)}}$ (162)	15	4.52	275	0.234	265
	$\pi_{3,\mathrm{DMA(6,8)}}$ (159)	$\rightarrow$	$\pi^*_{4,\mathrm{DMA(6,8)}}$ (166)	13				
	$\pi_{8,\mathrm{py}}$ (160)	$\rightarrow$	$\pi^*_{4,\mathrm{DMA(6,8)}}$ (166)	12				
			PyLa06					
S_1	$\pi_{8,\mathrm{py}}$ (160)	$\rightarrow$	$\pi^*_{9,\mathrm{py}} + \pi^*_{4,\mathrm{DMA(6)}}$ (161)	91	3.27	379	1.165	360
S_4	$\pi_{3,\mathrm{DMA(3,8)}}$ (158)	$\rightarrow$	$\pi^*_{9,\mathrm{py}} + \pi^*_{4,\mathrm{DMA(6)}}$ (161)	45	4.22	294	0.649	300
	$\pi_{8,\mathrm{py}}$ (160)	$\rightarrow$	$\pi^*_{4,\mathrm{DMA(6)}}$ (162)	26				
S_5	$\pi_{8,\mathrm{py}}$ (160)	$\rightarrow$	$\pi^*_{4,\mathrm{DMA(3,8)}}$ (165)	29	4.32	287	0.179	265
	$\pi_{3,\mathrm{DMA(3,8)}}$ (158)	$\rightarrow$	$\pi^*_{9,\mathrm{py}} + \pi^*_{4,\mathrm{DMA(6)}}$ (161)	22				
	$\pi_{8,\mathrm{py}}$ (160)	$\rightarrow$	$\pi^*_{4,\mathrm{DMA(6)}}$ (164)	21				
			PyLa08					
S_1	$\pi_{8,\mathrm{py}}$ (160)	$\rightarrow$	$\pi^*_{9,\mathrm{py}} + \pi^*_{4,\mathrm{DMA(8)}}$ (161)	91	3.28	378	1.095	360
S_3	$\pi_{3,\mathrm{DMA(3,6)}}$ (159)	$\rightarrow$	$\pi^*_{9,\mathrm{py}} + \pi^*_{4,\mathrm{DMA(8)}}$ (161)	73	4.07	304	0.649	300
S_8	$\pi_{6,\mathrm{py}}$ (157)	$\rightarrow$	$\pi^*_{9,\mathrm{py}} + \pi^*_{4,\mathrm{DMA(8)}}$ (161)	19	4.59	270	0.225	265
	$\pi_{8,\mathrm{py}}$ (160)	$\rightarrow$	$\pi^*_{5,\mathrm{DMA(3,6)}}$ (168)	18				
	$\pi_{7,\mathrm{py}} + \pi_{3,\mathrm{DMA(3,6)}}$ (158)	$\rightarrow$	$\pi^*_{10,\mathrm{py}}$ (165)	9				
	$\pi_{3,\mathrm{DMA(3,6)}}$ (159)	$\rightarrow$	$\pi^*_{4,\mathrm{DMA(3,6)}}$ (166)	9				

Table S4 Calculated vertical excitation energies (E), oscillator strengths (f) and main single-excited configurations of the main excited states of the mono-protonated forms of PyLa at B3LYP/TZVP//CAM-B3LYP/TZVP (IEFPCM of acetonitrile) as level of theory and experimental absorption maxima.

S_n	transition			p	E	λ	f	$\lambda^{\text{Exp.}}$
				in %	in eV	in nm		in nm
			PyLa13					
S_1	$\pi_{8,\text{py}}$ (160)	$\rightarrow$	$\pi^*_{9,\text{py}}$ (161)	89	3.00	413	0.981	417
S_3	$\pi_{8,\text{py}}$ (160)	$\rightarrow$	$\pi^*_{4,\text{DMA(3)}}$ (162)	33	3.77	329	0.250	300
	$\pi_{3,\text{DMA(6,8)}}$ (159)	$\rightarrow$	$\pi^*_{9,\text{py}}$ (161)	23				
	$\pi_{7,\text{py}}$ (157)	$\rightarrow$	$\pi^*_{9,\text{py}}$ (161)	19				
S_6	$\pi_{7,\text{py}}$ (157)	$\rightarrow$	$\pi^*_{9,\text{py}}$ (161)	42	4.45	279	0.545	265
	$\pi_{8,\text{py}}$ (160)	$\rightarrow$	$\pi^*_{4,\text{DMA(3)}}$ (162)	25				
			PyLa16					
S_1	$\pi_{8,\text{py}}$ (160)	$\rightarrow$	$\pi^*_{9,\text{py}}$ (161)	90	3.03	409	1.027	417
S_4	$\pi_{3,\text{DMA(3,8)}}$ (158)	$\rightarrow$	$\pi^*_{9,\text{py}}$ (161)	74	4.03	308	0.474	300
S_6	$\pi_{7,\text{py}}$ (157)	$\rightarrow$	$\pi^*_{9,\text{py}}$ (161)	42	4.47	277	0.632	265
	$\pi_{8,\text{py}}$ (160)	$\rightarrow$	$\pi^*_{4,\text{DMA(6)}}$ (162)	32				
			PyLa18					
S_1	$\pi_{8,\text{py}}$ (160)	$\rightarrow$	$\pi^*_{9,\text{py}}$ (161)	89	3.03	409	1.002	417
S_3	$\pi_{3,\text{DMA(3,6)}}$ (159)	$\rightarrow$	$\pi^*_{9,\text{py}}$ (161)	32	3.81	325	0.255	300
	$\pi_{8,\text{py}}$ (160)	$\rightarrow$	$\pi^*_{4,\text{DMA(8)}}$ (162)	27				
	$\pi_{7,\text{py}}$ (157)	$\rightarrow$	$\pi^*_{9,\text{py}}$ (161)	16				
S_6	$\pi_{7,\text{py}}$ (157)	$\rightarrow$	$\pi^*_{9,\text{py}}$ (161)	48	4.45	279	0.632	265
	$\pi_{8,\text{py}}$ (160)	$\rightarrow$	$\pi^*_{4,\text{DMA(8)}}$ (162)	38				
			PyLa136					
S_1	$\pi_{8,\text{py}}$ (160)	$\rightarrow$	$\pi^*_{9,\text{py}}$ (161)	87	3.32	374	1.046	386
S_3	$\pi_{3,\text{DMA(3,6)}}$ (159)	$\rightarrow$	$\pi^*_{9,\text{py}}$ (161)	74	4.11	302	0.301	300
S_6	$\pi_{8,\text{py}}$ (160)	$\rightarrow$	$\pi^*_{4,\text{DMA(8)}}$ (162)	43	4.50	276	0.480	265
	$\pi_{7,\text{py}}$ (158)	$\rightarrow$	$\pi^*_{9,\text{py}}$ (161)	20				
			PyLa138					
S_1	$\pi_{8,\text{py}}$ (160)	$\rightarrow$	$\pi^*_{9,\text{py}}$ (161)	88	3.32	373	0.999	386
S_3	$\pi_{3,\text{DMA(3,8)}}$ (159)	$\rightarrow$	$\pi^*_{9,\text{py}}$ (161)	76	4.12	301	0.352	300
S_6	$\pi_{7,\text{py}}$ (158)	$\rightarrow$	$\pi^*_{9,\text{py}}$ (161)	38	4.52	274	0.649	265
	$\pi_{8,\text{py}}$ (160)	$\rightarrow$	$\pi^*_{4,\text{DMA(6)}}$ (163)	22				
			PyLa168					
S_1	$\pi_{8,\text{py}}$ (160)	$\rightarrow$	$\pi^*_{9,\text{py}}$ (161)	87	3.29	377	1.055	386
S_3	$\pi_{3,\text{DMA(6,8)}}$ (159)	$\rightarrow$	$\pi^*_{9,\text{py}}$ (161)	66	4.09	303	0.344	300
S_6	$\pi_{8,\text{py}}$ (160)	$\rightarrow$	$\pi^*_{4,\text{DMA(3)}}$ (164)	17	4.63	268	0.382	265
	$\pi_{7,\text{py}}$ (157)	$\rightarrow$	$\pi^*_{9,\text{py}}$ (161)	17				

Table S5 Calculated vertical excitation energies (E), oscillator strengths (f) and main single-excited configurations of the main excited states of the di-protonated forms of PyLa at B3LYP/TZVP//CAM-B3LYP/TZVP (IEFPCM of acetonitrile) as level of theory and experimental absorption maxima.

S_n	transition			p	E	λ	f	$\lambda^{\text{Exp.}}$
				in %	in eV	in nm		in nm
			PyLa236					
S_1	$\pi_{8,\text{py}}$ (160)	$\rightarrow$	$\pi^*_{9,\text{py}}$ (161)	83	3.08	402	0.929	417
S_3	$\pi_{3,\text{DMA(8)}}$ (159)	$\rightarrow$	$\pi^*_{9,\text{py}}$ (161)	61	3.82	325	0.202	370
S_5	$\pi_{7,\text{py}}$ (158)	$\rightarrow$	$\pi^*_{9,\text{py}}$ (161)	42	4.45	279	0.721	265
	$\pi_{8,\text{py}}$ (160)	$\rightarrow$	$\pi^*_{4,\text{DMA(3,6)}}$ (162)	37				
			PyLa238					
S_1	$\pi_{8,\text{py}}$ (160)	$\rightarrow$	$\pi^*_{9,\text{py}}$ (161)	84	3.09	401	0.942	417
S_3	$\pi_{3,\text{DMA(6)}}$ (159)	$\rightarrow$	$\pi^*_{9,\text{py}} + \pi^*_{\text{COO}}$ (161)	49	3.91	317	0.272	370
	$\pi_{8,\text{py}}$ (160)	$\rightarrow$	$\pi^*_{4,\text{DMA(3,8)}}$ (162)	14				
S_5	$\pi_{7,\text{py}}$ (158)	$\rightarrow$	$\pi^*_{9,\text{py}}$ (161)	45	4.46	278	0.614	265
	$\pi_{8,\text{py}}$ (160)	$\rightarrow$	$\pi^*_{4,\text{DMA(3,8)}}$ (162)	39				
			PyLa268					
S_1	$\pi_{8,\text{py}}$ (160)	$\rightarrow$	$\pi^*_{9,\text{py}}$ (161)	84	3.11	399	0.905	417
S_3	$\pi_{3,\text{DMA(3)}}$ (159)	$\rightarrow$	$\pi^*_{9,\text{py}}$ (161)	58	3.85	322	0.157	370
S_5	$\pi_{8,\text{py}}$ (160)	$\rightarrow$	$\pi^*_{4,\text{DMA(6,8)}}$ (162)	36	4.47	278	0.609	265
	$\pi_{7,\text{py}}$ (158)	$\rightarrow$	$\pi^*_{9,\text{py}}$ (161)	34				

Table S6 Calculated vertical excitation energies (E), oscillator strengths (f) and main single-excited configurations of the main excited states of the tri-protonated forms of PyLa at B3LYP/TZVP//CAM-B3LYP/TZVP (IEFPCM of acetonitrile) as level of theory and experimental absorption maxima.

S_n	transition			p	E	λ	f	$\lambda^{\text{Exp.}}$
				in %	in eV	in nm		in nm
			PyLa31					
S_1	$\pi_{8,\text{py}}$ (160)	$\rightarrow$	$\pi^*_{9,\text{py}}$ (161)	95	3.33	373	0.967	370
S_3	$\pi_{5,\text{py}}$ (157)	$\rightarrow$	$\pi^*_{9,\text{py}}$ (161)	55	4.53	274	0.258	300
S_4	$\pi_{8,\text{py}}$ (160)	$\rightarrow$	$\pi^*_{4,\text{DMA(3,6,8)}}$ (163)	48	4.56	272	0.279	265
	$\pi_{8,\text{py}}$ (160)	$\rightarrow$	$\pi^*_{11,\text{py}}$ (169)	15				
S_5	$\pi_{8,\text{py}}$ (160)	$\rightarrow$	$\pi^*_{10,\text{py}}$ (162)	26	4.62	268	0.614	265
	$\pi_{5,\text{py}}$ (157)	$\rightarrow$	$\pi^*_{9,\text{py}}$ (161)	23				
	$\pi_{7,\text{py}}$ (159)	$\rightarrow$	$\pi^*_{9,\text{py}}$ (161)	18				

Additional Photophysical Characterisation

Table S7 Photophysical data including UV-Vis absorption maxima (λ_{abs} nm), emission maxima (λ_{em} nm), full width half maximum of emission intensity profile (FWHM), quantum fluorescence yield of the charge-transfer emission (ϕ_{fl}) and luminescent lifetime (τ_{lum} ns) of PyLa and PyLaOT in a range of different solvents. [a]Previously reported in literature.

	Solvent	λ_{abs} (nm)	λ_{em} (nm)	FWHM (cm^{-1})	ϕ_{fl}	τ_{lum} (ns)
	1-butanol	397	487	3226	0.11	2.7
	2-propanol	396	486	4676	0.27	2.4
	Chloroform	437	537	2674	0.88	3.1
	Ethanol	396	500	3471	0.82	3.2
PyLa	Tetrahydrofuran	419	501	4290	0.88	3.1
	Methanol	396[a]	525[a]	3696	0.55	3.5[a]
	Acetone	426[a]	580[a]	3338	0.97	2.6[a]
	Acetonitrile	399[a]	520[a]	3620	0.49[a]	3.8[a]
	Dichloromethane	431[a]	552[a]	2965	0.40[a]	4.4[a]
	1-butanol	404	523	3652	0.15	2.7
	2-propanol	404	524	3699	0.89	2.1
	Chloroform	394	510	3001	0.99	2.5
	Ethanol	404	530	3913	0.99	2.5
PyLaOT	Tetrahydrofuran	407	508	3393	0.12	2.6
	Methanol	398	550	3767	0.67	2.2
	Acetone	411	530	3728	0.99	
	Acetonitrile	416	552	3660	0.31	4.6
	Dichloromethane	410	515	3136	0.73	2.6

Table S8 Photophysical data (λ_{abs} nm), emission maxima (λ_{em} nm) and luminescent lifetime (τ ns) of PyLa and PyLaOT in PBS and acetonitrile at isolated pH.

		pH 7.4			**pH 5.5**			**pH 4.4**			**pH 1.5**			**pH Reversal**		
	Solvent	**(Neutral Species)**			**(Mono-)**			**(Di-)**			**(Tris-)**			**(Addition of base)**		
		λ_{abs} (nm)	λ_{em} (nm)	τ (ns)	λ_{abs} (nm)	λ_{em} (nm)	τ (ns)	λ_{abs} (nm)	λ_{em} (nm)	τ (ns)	λ_{abs} (nm)	λ_{em} (nm)	τ (ns)	λ_{abs} (nm)	λ_{em} (nm)	τ (ns)
PyLa	**PBS**	417	577	2.74±0.10	434	575	2.46 ± 0.10	444	575	2.28 ± 0.11	380	450	2.20±0.06	420	552	2.5 ± 0.05
	ACN	404	518	3.79 ±0.02	408	518	3.77 ± 0.05	380	433	1.51 ± 0.01	379	433	2.69 ± 0.1	413	565	1.52±0.01
PyLaOT	**PBS**	434	544	3.80 ±0.15	438	542	3.33 ±0.14	438	544	2.79 ± 0.06	378	428	2.25±0.01	434	532	2.65±0.07
	ACN	418	550	4.67 ± 0.05	418	520	5.44 ± 0.06	384	430	4.74 ± 0.01	378	430	2.77±0.01	418	560	3.95±0.01

*EDT microprocessor pH meter was used to measure pH in PBS samples with changes in pH due to HCl and NaOH titrations. In acetonitrile we refer to pH approximation; pH -log[$HClO_4$] as perchloric acid and triethylamine was used to determine apparent pH.

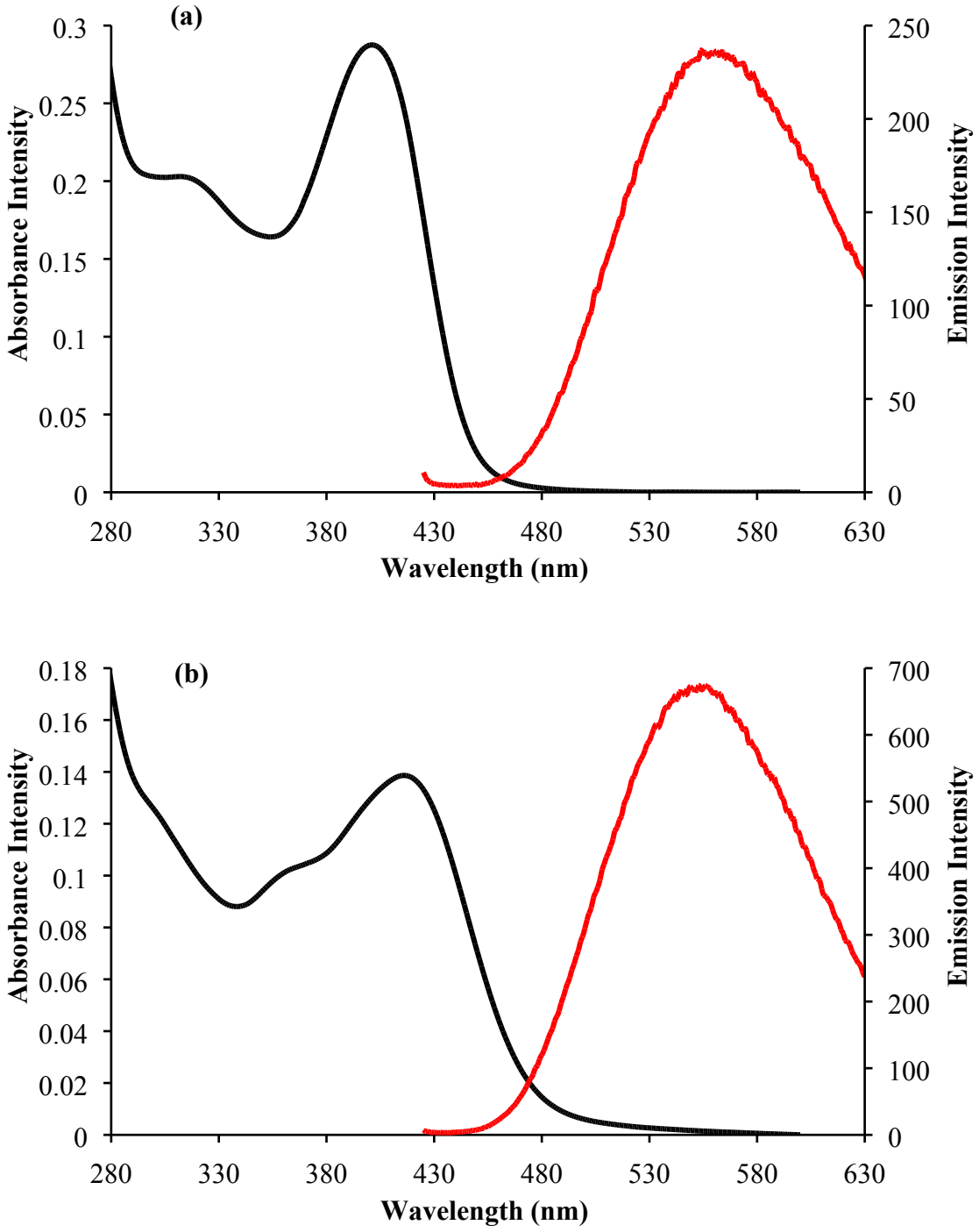

Figure S8 Absorbance and emission spectra of PyLa **(a)** and PyLaOT **(b)** in acetonitrile (sample concentration 20 µM). Emission spectra were obtained using slit widths of 5 nm.

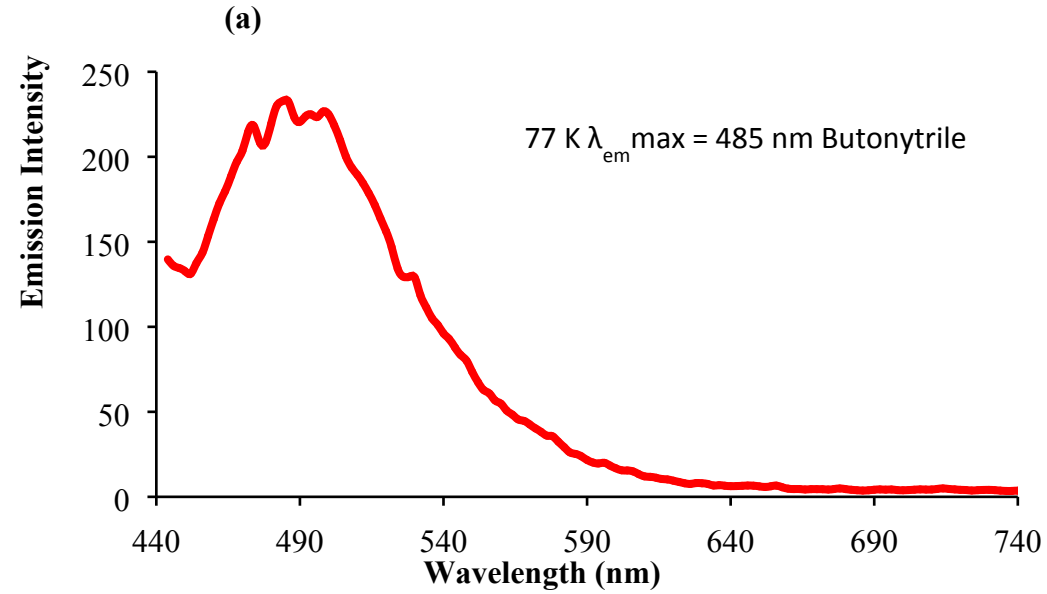
(a)
Emission Intensity
250
200
150
100
50
0
77 K λem max = 485 nm Butonytrile
440
490
540
590
640
690
740
Wavelength (nm)

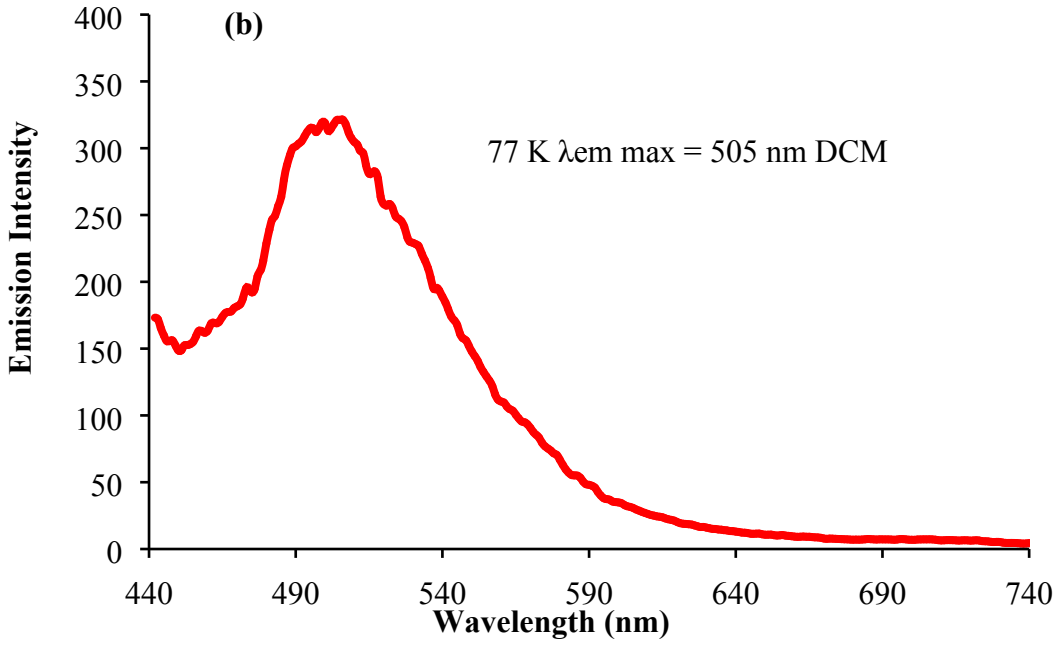
(b)
Emission Intensity
400
350
300
250
200
150
100
50
0
77 K λem max = 505 nm DCM
440
490
540
590
640
690
740
Wavelength (nm)

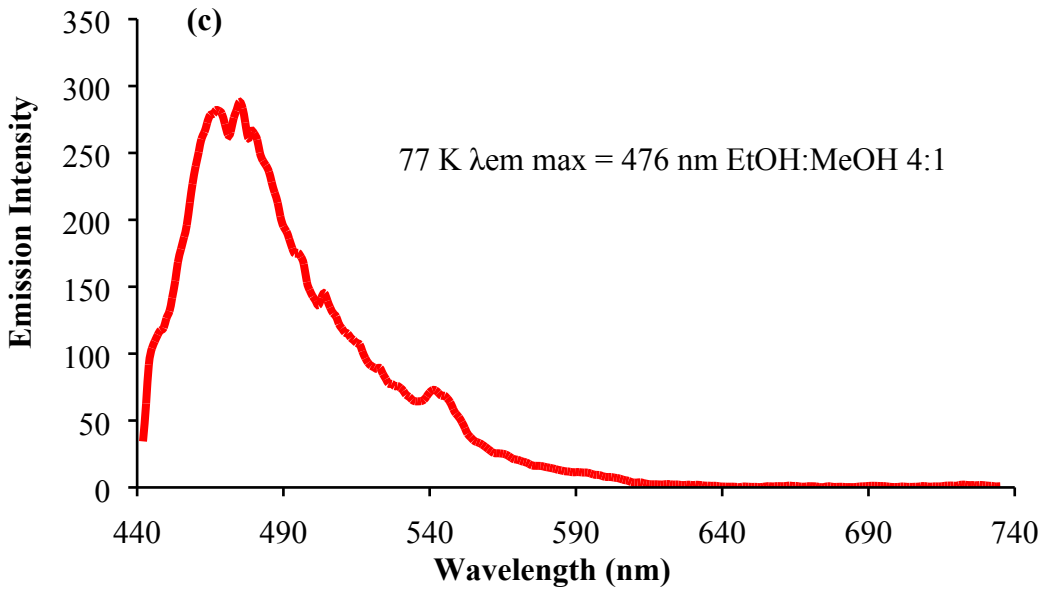

Figure S9 77 K emission spectra of PyLa in butonytrile **(a)**, dichloromethane **(b)** and ethanol:methanol 4:1: **(c)** (sample concentration 1 μM). Emission spectra were obtained using an excitation slit width of 5 nm and emission slit width of 10 nm.

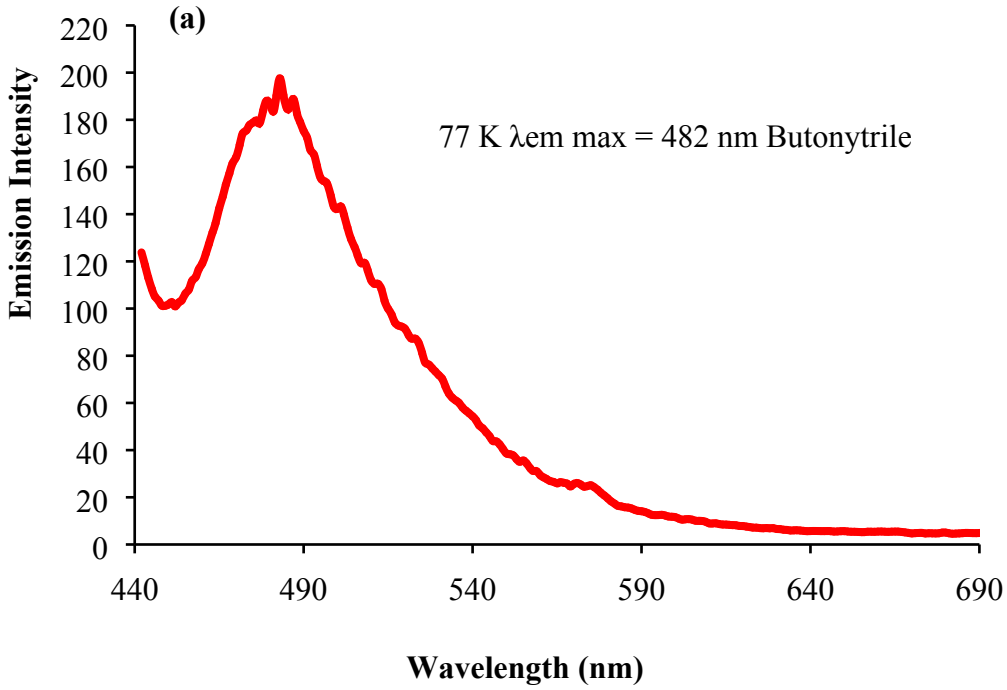

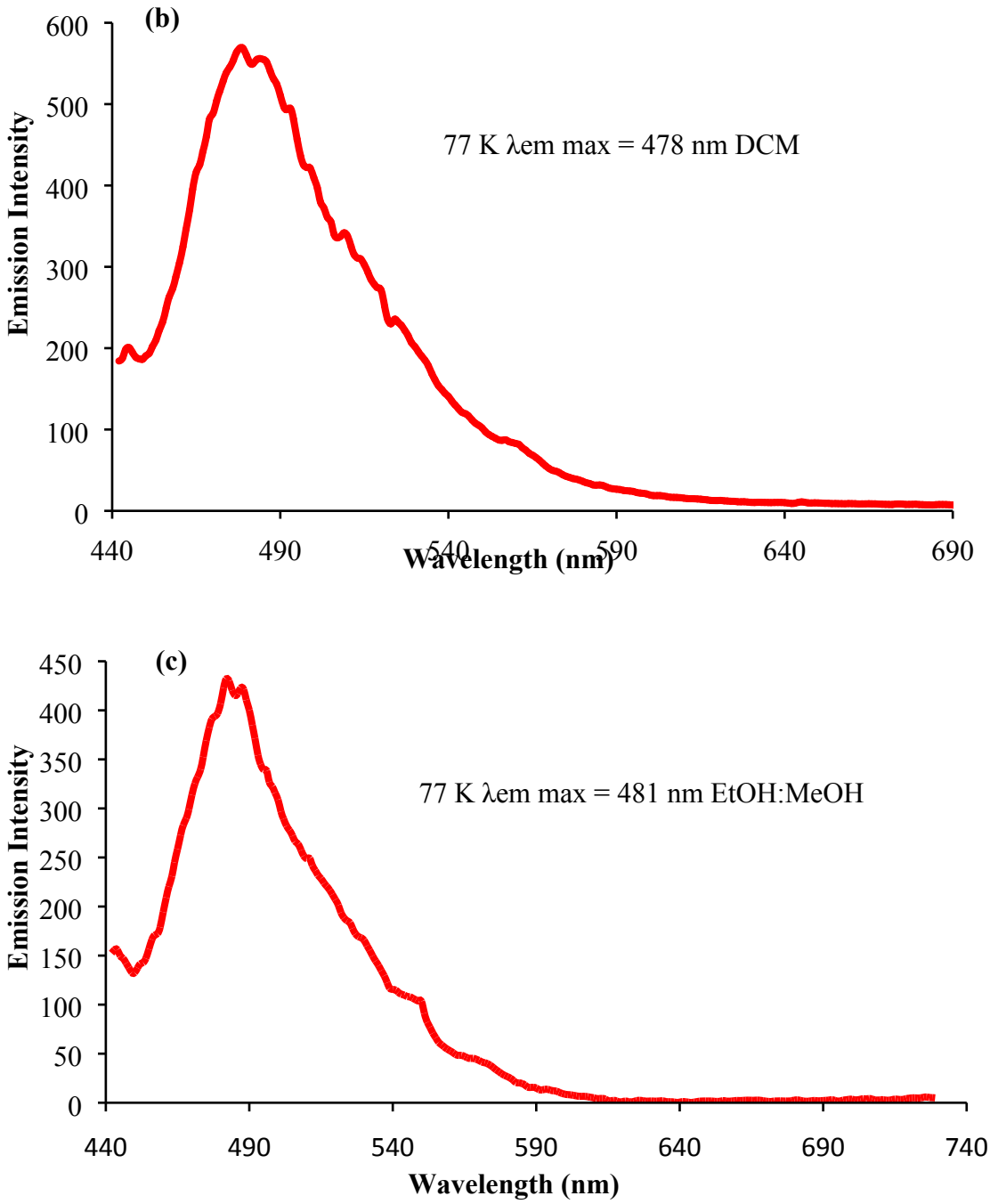

Figure S10 77 K emission spectra of PyLa-OT in butonytrile **(a)**, dichloromethane **(b)** and ethanol:methanol 4:1: **(c)** (sample concentration 1 μM). Emission spectra were obtained using an excitation slit width of 5 nm and emission slit width of 10 nm.

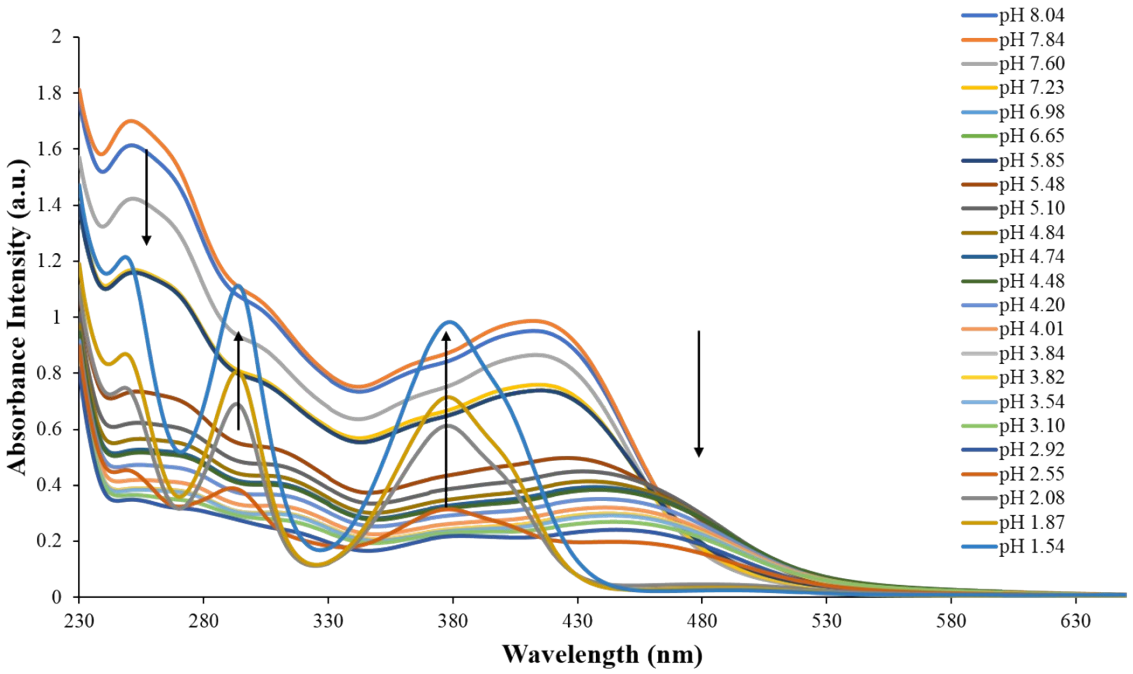

Figure S11 Absorption spectra of PyLa at decreasing pH values (c = 100 µM) in PBS. Spectra shows decrease in absorbance max and red-shift at approximately 428 nm with decreasing pH. Disappearance of this absorbance shoulder is observed below pH 3 with the formation of a pyrene like absorbance max at approximately 380 nm which then increases in intensity with decreasing pH.

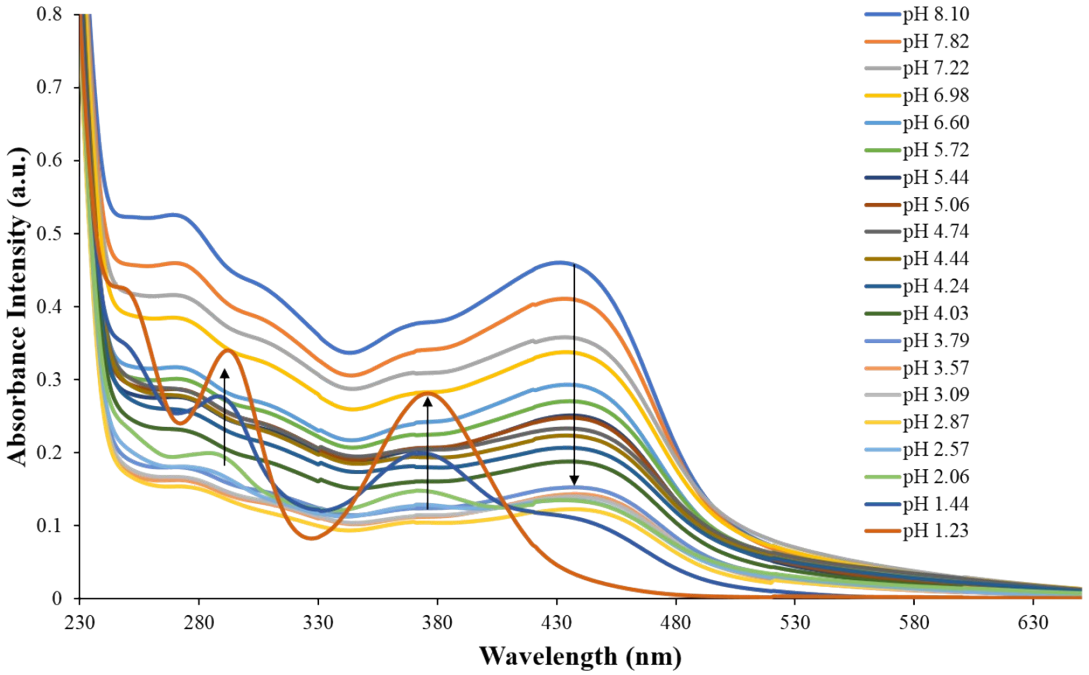

Figure S12 Absorption spectra of PyLaOT at decreasing pH values (c = 100 µM) in PBS. Spectra shows decrease in absorbance max and red-shift at approximately 434 nm with decreasing pH.

Disappearance of this absorbance shoulder is observed below pH 3 with the formation of a pyrene like absorbance max at approximately 380 nm which then increases in intensity with decreasing pH.

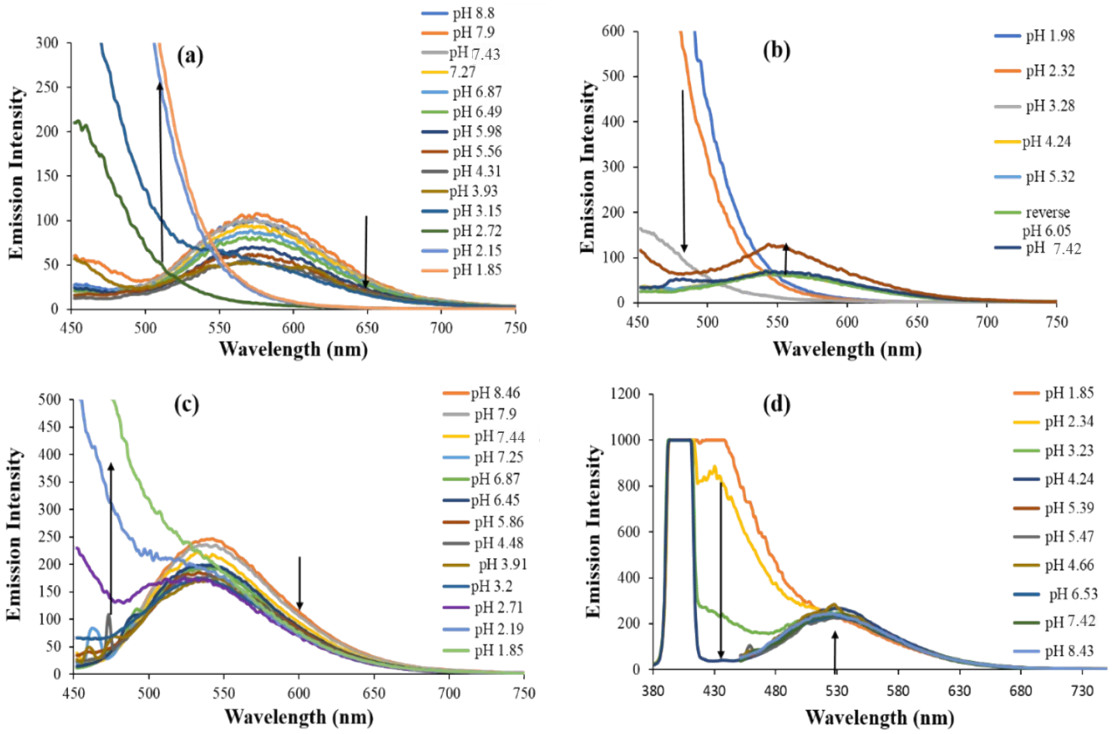

Figure S13 (a) Emission spectra of PyLa at decreasing pH values (c = 100 µM) in PBS. (b) Emission spectra of PyLa at increasing pH values (c = 100 µM) in PBS. (c) Emission spectra of PyLa-OT at decreasing pH values (c = 100 µM) in PBS. (d) Emission spectra of PyLa-OT at increasing pH values (c = 100 µM) in PBS. PyLa = λ_{Ex} 384 nm, PyLaOT = λ_{Ex} 398 nm.

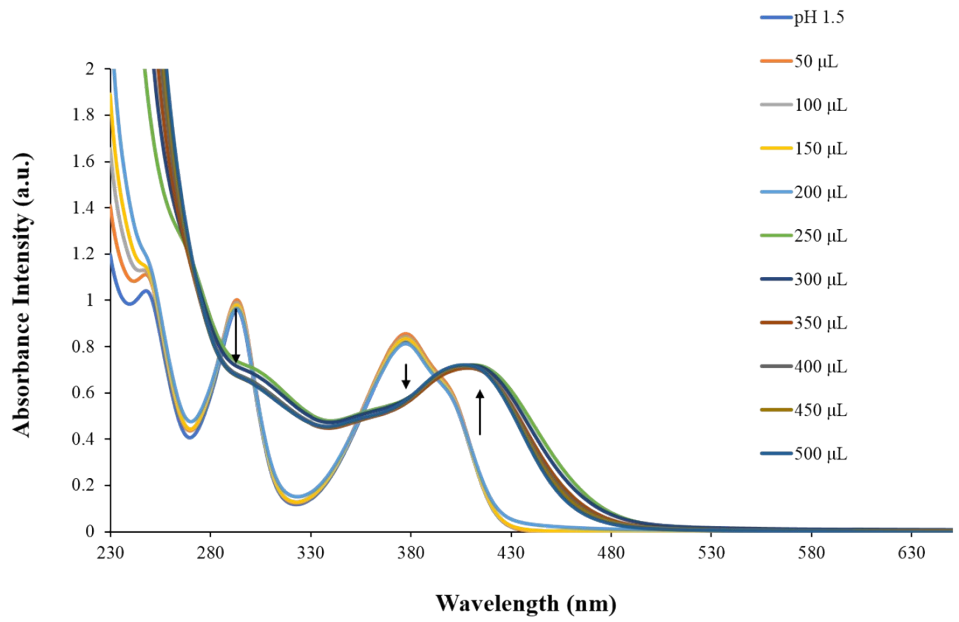

Figure S14 Absorption spectra of PyLa at increasing pH values (c = 50 µM) in acetonitrile using titrations of triethylamine. At pH 1.5 the absorbance max of PyLa is approximately 378 nm. This absorbance max slightly decreases with addition of triethylamine until the addition of 250 µL, at which point the normal absorbance max of approximately 420 nm is restored.

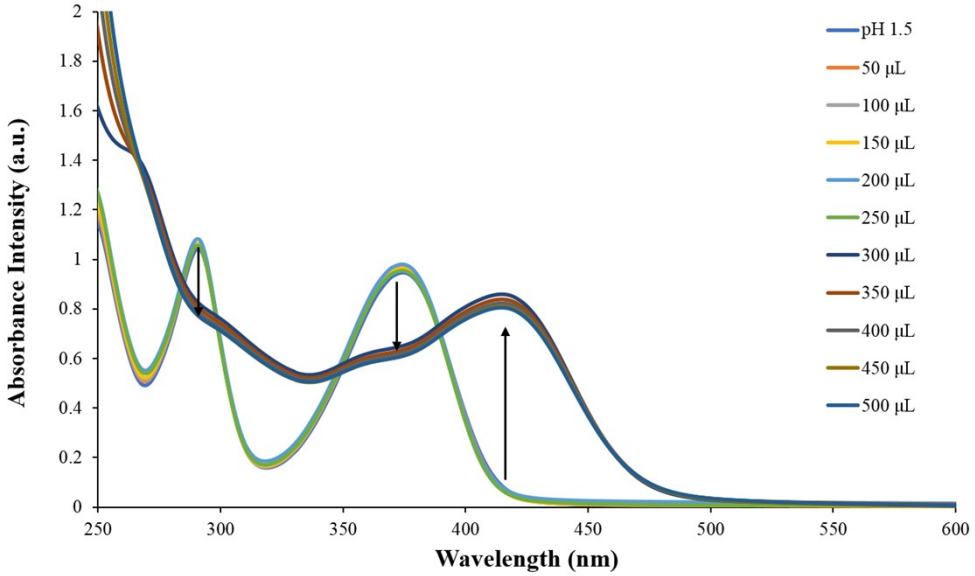

Figure S15 Absorption spectra of PyLa at increasing pH values (c = 50 µM) in acetonitrile using titrations of triethylamine. At pH 1.5 the absorbance max of PyLa is approximately 376 nm. This absorbance decreases slightly with addition of triethylamine until the addition of 300 µL, at which point the normal absorbance max of approximately 418 nm is restored.

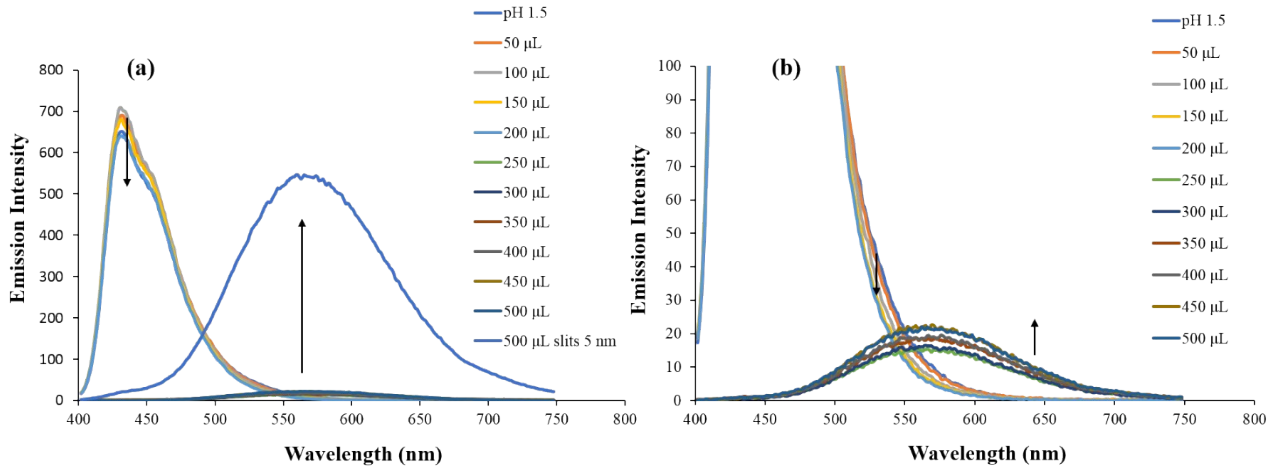

Figure S16 (a) Emission spectra of PyLa at increasing pH values (c = 50 µM) in acetonitrile using titrations of triethylamine, excited at 384 nm. At pH 1.5 the emission maxima of PyLa is approximately 430 nm. This decreases in intensity with increasing pH. After the addition of 250 µL of triethylamine the charge-transfer emission band at 520 nm is restored and increases slightly with increasing pH. Excitation slit width was 2.5 nm and emission slit width was 5 nm. and the emission is show after the addition of 500 µL with excitation and emission slit widths set to 5 nm also. (b) Inset of the appearance of the charge-transfer emission band at 520 nm after the addition of 250 µL and the slight increase in emission intensity with the addition of triethylamine.

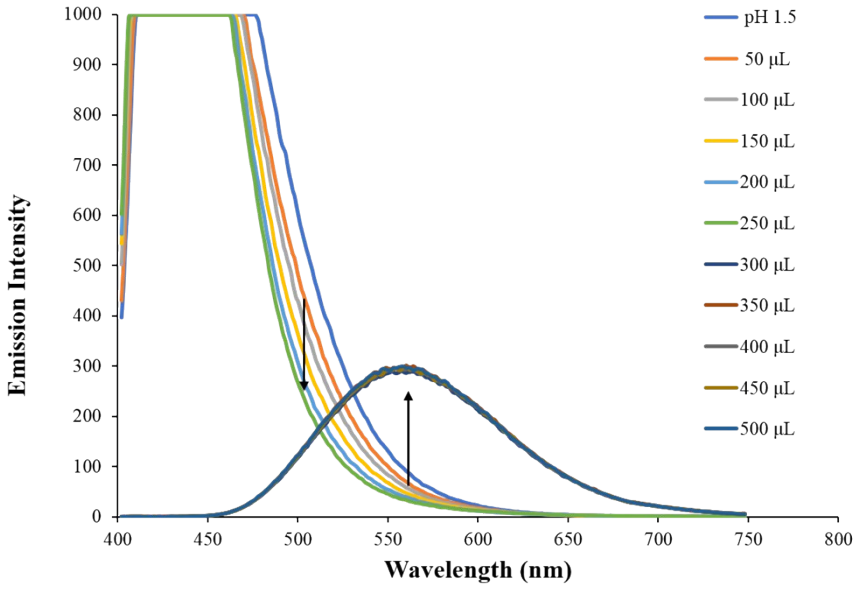

Figure S17 (a) Emission spectra of PyLaOT at increasing pH values (c = 50 µM) in acetonitrile on addition of triethylamine, exciting at 392 nm. At pH 1.5 the emission maxima of PyLaOT is approximately 426 nm. This decreases in intensity with increasing pH. After the addition of 300 µL of triethylamine the charge-transfer emission band at 552 nm is restored. Excitation and emission slit widths were 2.5 nm and 5 nm respectively.

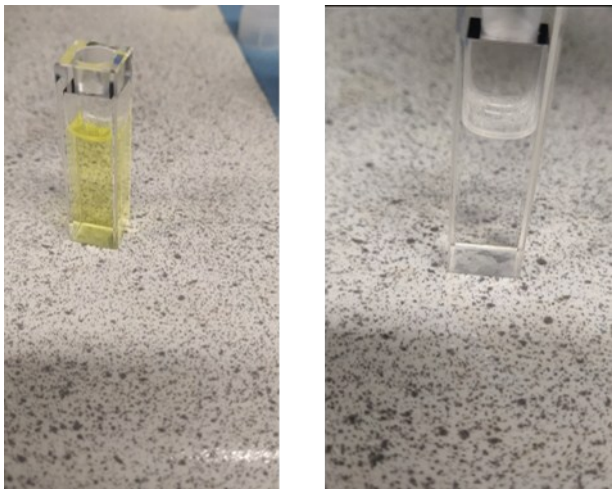

Figure S18 (a) Solution of PyLa (c = 50 µM) in acetonitrile (luminescent yellow). (b) Solution of PyLa (c = 50 µM) in acetonitrile upon addition of triethylamine (pH > 3) (colourless). The colour of the solution changes from luminescent yellow to colourless. This reversible colour change occurs for both PyLa and PyLaOT in both PBS and acetonitrile.

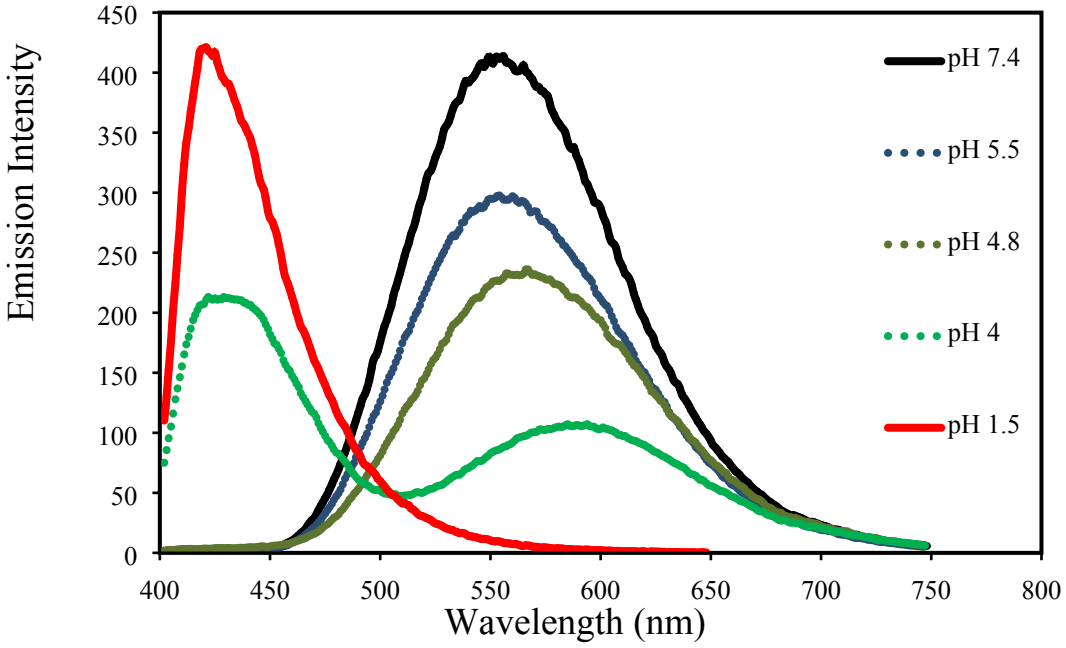

Figure S19 Emission spectra of PyLaOT (c = 50 µM) in acetonitrile. pH (7.5-4) were excited into the absorbance max at approximately 409 nm using excitation and emission slit widths of 5 nm and 2.5 nm respectively. pH 1.5 was excited into the absorbance max at approximately 378 nm and slit widths were reduced to 2.5 nm in order show full emission profile without saturating the detector.